**Paper:**
Dhas, C., Christy, A., Venkatesh, R., S., E., Panda, S., Subramanian, B., Ravichandran, K., Sudhagar, P. & Raj, A. (2018). Low-cost and eco-friendly nebulizer spray coated CuInAlS 2 counter electrode for dye-sensitized solar cells. *Physica B: Condensed Matter, 537*, 23-32.
http://dx.doi.org/10.1016/j.physb.2018.01.042

# Accepted Manuscript

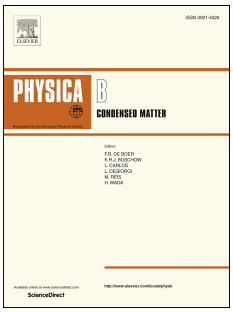


Low-cost and eco-friendly nebulizer spray coated $CuInAlS_2$ counter electrode for dye-sensitized solar cells

C. Ravi Dhas, A. Jennifer Christy, R. Venkatesh, S. Esther Santhoshi Monica, Subhendu K. Panda, B. Subramanian, K. Ravichandran, P. Sudhagar, A. Moses Ezhil Raj

PII: S0921-4526(18)30072-3

DOI: 10.1016/j.physb.2018.01.042

Reference: PHYSB 310689

To appear in: *Physica B: Physics of Condensed Matter*

Received Date: 19 October 2017

Revised Date: 11 December 2017

Accepted Date: 17 January 2018

Please cite this article as: C.R. Dhas, A.J. Christy, R. Venkatesh, S.E.S. Monica, S.K. Panda, B. Subramanian, K. Ravichandran, P. Sudhagar, A.M.E. Raj, Low-cost and eco-friendly nebulizer spray coated $CuInAlS_2$ counter electrode for dye-sensitized solar cells, *Physica B: Physics of Condensed Matter* (2018), doi: 10.1016/j.physb.2018.01.042.

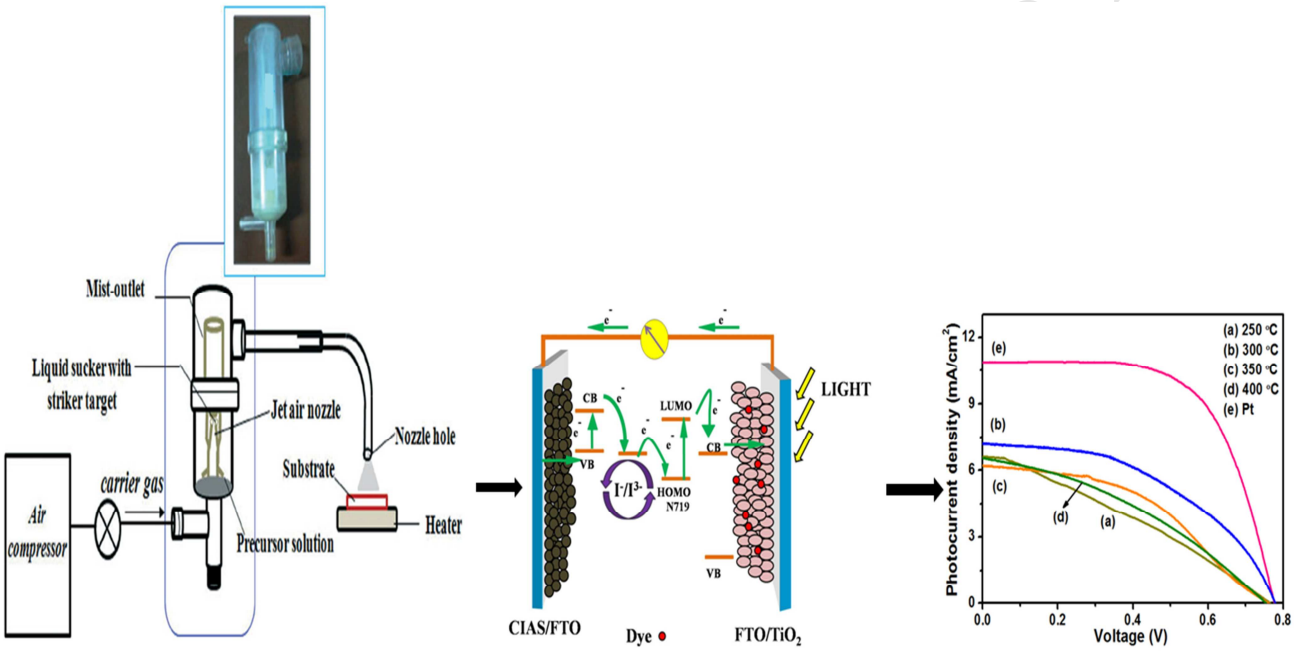

**sensitized solar cells**

**C. Ravi Dhas[1*], A. Jennifer Christy[1], R.Venkatesh[1], S. Esther Santhoshi Monica[1], Subhendu K. Panda[2*], B. Subramanian[2], K.Ravichandran[3], P.Sudhagar[4], A. Moses Ezhil Raj[5]**

[1]PG & Research Department of Physics, Bishop Heber College (Autonomous), Tiruchirappalli-620 017, Tamil Nadu, India

[2]CSIR-Central Electrochemical Research Institute (CECRI), Karaikudi-630 006, India

[3]Department of Physics, AVVM Sri Pushpam College, (Autonomous), Poondi, Thanjavur-613 503, Tamil Nadu, India

[4]Photocatalyst and Coatings Group, SPECIFIC, College of Engineering, Swansea University (Bay Campus), Fabianway, Swansea SA1 8EN, United Kingdom

[5]Department of Physics, Scott Christian College, (Autonomous), Nagercoil-629 003, Tamil Nadu, India

* Corresponding author email addresses: ravidhasc@gmail.com and skpanda@ceci.res.in

**Corresponding Authors**

**Dr.C. Ravi Dhas**
Head and Assistant Professor,
PG & Research Department of Physics,
Bishop Heber College (Autonomous),
Tiruchirappalli-620 017, Tamil Nadu, India.
Mobile: +91 9443076209
Land line: 0431-2770136
Fax: 0431-2770293
e-mail: ravidhasc@gmail.com; cravidhas@gmail.com

**Dr. Subhendu Kumar Panda**
Scientist,
Central Electrochemical Research Institute (CECRI),
(CSIR-Council of Scientific and Industrial Research),
Karaikudi-630006, Tamil Nadu, India.
Office: +91 456 524 1234
e-mail: skpanda@cecri.res.in

$CuInAlS_2$ thin films for different substrate temperatures were deposited by a novel nebulizer spray technique. The polycrystalline CIAS thin film exhibited tetragonal structure with the preferential orientation of (1 1 2) plane. Nanoflakes were observed from the surface morphology of CIAS film. The peak position of core level spectra confirms the presence of $CuInAlS_2$ from XPS analysis. The absorbance spectra and optical band gap were observed from the optical property. The activation energy, carrier concentration, hole mobility and resistivity were determined by linear four probe and Hall effect measurements. The CIAS film was used as a counter electrode (CE) in dye-sensitized solar cells (DSSCs) and is characterized by cyclic voltammetry, electrochemical impedance spectroscopy and Tafel measurements. DSSC fabricated with the CIAS CE achieved the photo conversion efficiency of about 2.55 %.

**Key words:** CIAS, nebulizer spray, XPS, counter electrode, dye-sensitized solar cells.

## 1. Introduction

In recent days, the traditional fossil resources such as coal, petroleum, and natural gas have been scarce as the energy demand and global economy increased abundantly. Solar energy is the best alternative to the traditional fossil resources because of its non-pollution and renewability [1]. Dye-sensitized solar cells (DSSCs) have attracted research interests due to their low-cost, non-pollution, simple fabrication processes, high efficiency, etc [2]. The important part of DSSCs is the counter electrode (CE) whereas it should possess high electrocatalytic and electrical conductivity [3]. The high expensive, low natural abundance and poor corrosion resistance of platinum restrict the industrial use of DSSCs [4]. Therefore, an alternative low-cost

are widely used because of their strong electrocatalytic activity and stability in the tri-iodide process. Few reports are available for $CuInS_2$ (CIS) and $CuInGaS_2$ (CIGS) as CE material in DSSCs [5, 6].

$CuInS_2$ is one among the materials in chalcopyrite group which has high absorption co-efficient in the wide spectral range in the visible region, optimum optical energy band gap, good stability and radiation hardness [7]. $CuInS_2$ is one of the most potential candidates for the photovoltaic applications with the band gap value of 1.53 eV [8]. Moreover, in the quaternary material $CuInGaS_2$, gallium is a rare and expensive element, so it can be substituted by abundant and economical elements such as aluminum [9], iron [10], sodium [10], zinc [11], bismuth [12], titanium [13], cerium [14], tin [15], etc. Among these materials, Al is the most preferable material to be incorporated in $CuInS_2$ due to its corrosion resistance, good thermal and electrical conductivity. There are only a few records available in the literature for $CuInAlS_2$ [16-18]. Theoretically, the energy band gap of $CuInAlS_2$ (CIAS) can be varied from 1.53 eV ($CuInS_2$) to 3.5 eV ($CuAlS_2$) by tuning aluminum incorporation. CIAS thin films have been prepared mostly by PVD techniques such as thermal evaporation, sputtering followed by sulfurization at high temperature, etc [8, 9]. Since $H_2S$ gas is highly toxic and hazardous to human health, extra care has to be taken while using in the laboratory [19]. A simple and cheap method is required for manufacturing commercial solar cell devices on a large scale. Nebulizer spray method is simple, cost-effective and more advanced compared to conventional spray in preparing functional thin film coatings for different technical applications [20, 21]. The precise control of droplets size has the ability to produce good adherent, pinhole-free nanostructured film which is more advantageous over conventional spray method [22].

by a novel nebulizer spray technique for different substrate temperatures. The role of substrate temperature on the structural, morphological, electrical and optical properties of CIAS thin films was investigated. The electrocatalytic activity and the performance of device fabrication of CIAS CEs in DSSCs had been discussed in detail. We are the first to report the CIAS thin film prepared by nebulizer spray technique and also used as a CE in DSSCs.

## 2. Experimental

### *2.1. Preparation of CIAS thin film*

The working principle of nebulizer spray method had been reported earlier by our research group [23]. Copper (II) chloride dihydrate ($CuCl_2.2H_2O$), indium (III) chloride ($InCl_3$, anhydrous), aluminum (III) chloride ($AlCl_3$, anhydrous) and thiourea ($SC(NH_2)_2$) were purchased from Alfa Aesar and dissolved in distilled water for different substrate temperatures (250, 300, 350 and 400 °C) with the molar ratio of 1:0.7:0.3:4. The prepared solution was stirred vigorously at room temperature and sprayed onto clean glass and FTO substrates with the pressure of 1.0 $kg/cm^2$ to produce device quality of CIAS thin films.

### *2.2. Fabrication of DSSCs device*

All the assembled DSSCs were fabricated based on standard procedure using $TiO_2$ photoanode for fair comparison. FTO substrates were ultrasonically cleaned in ethanol, acetone and deionized water for 10 minutes to remove the contaminants over the surface. The cleaned FTO substrate was immersed in 20 mM aqueous solution of $TiCl_4$ to form $TiO_2$ blocking layer. The resultant film was gradually heated in air at 450 °C for 30 minutes. Commercial $TiO_2$ paste

obtain mesoporous and scattering layer which was baked at 150 °C for 5 minutes and finally annealed in air at 500 °C for 1 hour respectively. The obtained $TiO_2$ photoanode was soaked in a solution of N719 dye mixed with 0.3 mM of ethanolic solution for 12 hours at room temperature under dark condition. The excess dye molecules over $TiO_2$ photoanode were removed by dipping in ethanol and allowed to dry. The platinum CE layer on FTO was prepared by spin coating, the solution of $H_2PtCl_6.6H_2O$ dispersed in 10 mM isopropanol solution annealed at 400 °C for 30 minutes. The nebulizer-spray deposited CIAS/FTO CEs and Pt CE were separated using a surlyn film spacer with dye-sensitized $TiO_2$ electrode. The iodine electrolyte solution containing 0.06 M LiI, 0.6 M 1-propyl-2,3-dimethylimidazolium iodide, 0.03 M $I_2$, 0.5 M 4-tertbuyl pyridine and 0.1 M guanidinium thiocyanate dissolved in acetonitrile was injected in the gap between the two electrodes with a small capillary syringe and the holes were completely sealed with molten glue. The active area of the fabricated DSSCs was $0.4 \times 0.4$ $cm^2$.

*2.3. Characterization*

The deposited CIAS thin films were analyzed to study their structural, morphological, elemental composition, optical and electrical properties. The X-ray diffraction patterns were recorded with a PANanalytical X'PERT PRO diffractometer using Cu $K_\alpha$ radiation with a wavelength of 1.5406 Å. A Reinshaw (Invia Make) spectrometer was used to analyze the Raman spectra. The surface morphology of the film was analyzed by Scanning Electron Microscope (VEGA3 TESCAN) and Atomic Force Microscope (A100, APE Research). The chemical state of the CIAS thin film and its composition were investigated using Kratos axis ultra DLD X-ray photoelectron spectrometer and energy dispersive spectroscopy (Bruker). A JASCO UV-Vis-

Hall measurements were carried out by four probe method with the Keithley 2400 source meter and Ecopia HMS-3000 source meter respectively. The photocurrent density – voltage characterization of the prepared DSSCs was measured using a potentiostat (VMP3, BIO-LOGIC) under illumination using a solar simulator (Photoemission Tech) coupled with AM 1.5G filter set and the intensity of the illumination is 100 mW/cm$^2$. Cyclic voltammetric measurements were conducted using three electrode cells setup under iodine electrolyte. Pt wire was used as the counter electrode, standard calomel electrode (SCE) served as the reference electrode and CIAS/FTO as the working electrode. The electrochemical impedance spectroscopy (EIS) of prepared DSSCs was recorded at the constant potential of 0.7 V under dark condition in the frequency range 0.1 Hz to 1 MHz with an amplitude voltage of 10 mV.

## 3. Results and Discussion

### *3.1. X-ray diffraction analysis*

The structural developments of CIAS thin films are depicted as a function of substrate temperature which is shown in Fig.1. The as-deposited CIAS thin films were identified as tetragonal structure with the space group of I-42d. The diffraction peaks located at $2\theta$ = 27.8 °, 46.5 ° and 54.9 ° are assigned to (1 1 2), (2 0 4) and (2 1 5) planes respectively according to JCPDS card no 65-1572. The intensity of the polycrystalline CIAS thin film increases and full-width half maximum decreases with the increase in substrate temperature upto 300 °C giving an indication of enhancement in crystallinity. The reason may be the sufficient amount energy acquired by the atoms for diffusion in the crystal lattice. Further increasing the substrate temperature to 350 and 400 ºC, the intensity of the peaks deteriorates due to the re-evaporation

observed similar type of decline in peak intensity by increasing the substrate temperature beyond 300 ºC in Zn doped $CuInS_2$ films [25].

The different crystalline parameters of CIAS thin film like crystallite size (D), microstrain (ε), dislocation density (δ), and lattice parameters ('a' & 'c') are determined from the following the relations [21, 26],

$$D = \frac{K\,\lambda}{\beta \cos\theta} \quad (1)$$

$$\varepsilon = \frac{\beta \cos\theta}{4} \quad (2)$$

$$\delta = \frac{1}{D^2} \ (\text{lin}/\text{m}^2) \quad (3)$$

$$\frac{1}{\text{d}_{\text{hkl}}^2} = \frac{\text{h}^2 + \text{k}^2}{\text{a}^2} + \frac{\text{l}^2}{\text{c}^2} \quad (4)$$

where 'K' represents the shape factor taken as 0.9, 'λ' is the wavelength of X-ray (Kα=1.5406 Å), 'β' refers to full-width half maximum, 'θ' is the diffraction angle, 'd' denotes the distance between lattice points, and 'h', 'k', and 'l' represent to Miller indices.

Figure 2 represents the maximum crystallite size with the minimum microstrain and dislocation density obtained for the CIAS thin film deposited at 300 °C resulting in reduction in the concentration of lattice imperfections leading to preferred orientations [27]. The lattice parameters of CIAS thin film prepared for different substrate temperatures are listed in the Table

temperature in the prepared CIAS films as it is slightly deviated from Vegard's law. Basically in chalcopyrite type semiconductors $A^{I}B^{III}C_2^{VI}$, the tetragonal distortion is a vital parameter which is pure indication of unequal bond lengths between the A-C and B-C atoms [9]. The value of tetragonal distortion can be observed from c/a ratio (Fig. 3) with increase in substrate temperature and it follows a similar trend as X-ray diffraction intensity. This tetragonal distortion induces stress in the crystal structure which is directly reflected in crystalline parameters such as crystallite size, strain and dislocation density values of CIAS films. The lower crystallite size values observed for 350 and 400 °C might be due to small deviation in stochiometry as well as thermally generated defects increases the broadening of the diffraction peaks.

*3.2. Raman spectra*

Raman spectroscopy is a nondestructive tool to analyze the local structure from vibrational modes of the atoms present in the crystal lattice. Raman spectra of CIAS thin films were recorded at room temperature and the obtained results are shown in Fig. 4. In this work the peak obtained at 299 $cm^{-1}$ belongs to the $A_1$ mode of chalcopyrite structure observed for all the deposited CIAS thin films. On careful observation two important inferences can be observed: (i) the variation in peak broadening with substrate temperature and (ii) shift of $A_1$ mode towards larger wave number. The strong intense $A_1$ mode of chalcopyrite compounds in the Raman spectra generally located between the range 291-314 $cm^{-1}$ and in addition to $A_l$ mode another weak peak observed at 350 $cm^{-1}$ corresponds to $B_2$(LO) mode of chalcopyrite [9]. No other minor phases were observed in X-ray diffraction and it is once again confirmed in Raman

with less defect structure and can promote electron transfer at the CE/electrolyte interface [28].

*3.3. Surface morphology*

Figure 5 represents the SEM images of CIAS thin film deposited at different substrate temperatures. Small spherical grains are developed in the initial stage of nucleation process at 250 °C. When the substrate temperature increased to 300 °C, the grains began to grow into nanoflakes due to an adequate supply of the thermal energy. At high substrate temperatures (350 and 400 °C), the agglomerated grains resulted due to the formation of bigger islands as the mobility of surface atoms increases with the impact of high thermal energy applied to the substrate. Similar type of observation was made by Swapna et al. for spray pyrolyzed Mo doped zinc oxide thin films [29]. Thus the substrate temperature plays a vital role in determining the surface morphology and the morphology inturn affects the charge transport CE/electrolyte interface in DSSCs.

*3.4. Atomic force microscope (AFM)*

The surface topography of CIAS thin films was analyzed by AFM and the 2D and 3D AFM images of CIAS films prepared at different substrate temperatures are shown in Fig. 6. The obtained root mean square (rms) roughness values are reported in Table 1. AFM images reveal that grain growth depends on the substrate temperature. Initially at 250 °C, small and non-uniform grains are clearly visualized. CIAS film deposited at 300 °C seems to be dense and uniformly packed grains. The CIAS films deposited at 350 and 400 °C consist of some voids and cluster grain formation due to thermally generated defect structure at grain boundaries. The voids

poor performance in DSSCs. Generally for a CE material, the surface should be void-free for better electrical conductivity and electrocatalytic performance [30].

*3.5. X-ray photoelectron spectroscopy (XPS)*

Figure 7 (i) shows the XPS survey spectrum of CIAS thin film deposited at 300 °C in a wide energy range of 0 – 1200 eV. The characteristic peaks observed from survey spectra are Cu 2p, In 3p, O 1s, In 3d, C 1s, S 2p, Al 2s, Al 2p, and S 3s indicating the presence of elements in the prepared film. No other peaks related to impurities or secondary phases other than copper, indium, aluminum and sulfur were detected confirming the purity of elements. The obtained binding energy values of Cu, In, Al and S are reported in the literature [18]. The binding energy of carbon species C 1s (284.1 eV) was utilized to calibrate the spectra.

The core level spectra of copper, indium, aluminum and sulfur of CIAS thin film are displayed in Fig.7 (ii). The binding energy of copper peaks 931.2 and 950.0 eV corresponding to $2p_{3/2}$ and $2p_{1/2}$ respectively was split by 19.8 eV representing the Cu (I) oxidation state. Perera et al. reported a satellite peak at 942 eV that denotes Cu (II) oxidation state of $2p_{3/2}$ [31]. The nebulizer spray-coated CIAS thin film clearly represented the absence of Cu (II) state and confirmed the Cu (I) state. The indium peak $3d_{5/2}$ and $3d_{3/2}$ emerged at 444.5 and 452.1 eV with the splitting binding energy of 7.6 eV. A peak at 74.07 and 160.0 eV indicates Al 2p and S $2p_{3/2}$. The presence of oxygen (530.1 eV) and sulfur (167.8 eV) peaks were owing to the formation of sulphate as surface contaminant [32].

The EDS spectrum of CIAS thin film prepared at 300 °C is shown in Fig.8. The presence of copper, indium, aluminum and sulfur proved that no other impurities were present in the nebulizer spray-coated CIAS thin film. The elemental composition of CIAS thin films deposited at different substrate temperatures (inset of Table in Fig. 8) revealed better stoichiometric ratio.

*3.7. Optical properties*

Figure 9 shows the optical absorbance spectra of CIAS thin films deposited at different substrate temperatures measured in the wavelength range of 350 -1100 nm. A wide range of absorbance spectra was observed in the visible region for the all the deposited CIAS thin films and the absorbance decreases with the rise in the substrate temperature.

The optical band gap energy of the CIAS thin film deposited for different substrate temperatures can be obtained by using the Tauc plot relation [23],

$$\alpha h\nu = A\left(h\nu - E_g\right)^n \qquad (5)$$

where, '$\alpha$'- absorption co-efficient, '$h\nu$'- incident photon energy, '$E_g$' - band gap and 'n'- type of transition. CIAS is a direct band gap semiconducting material, therefore the value of 'n'=1/2. From Fig.10, the band gap energy values can be determined by extrapolating tangents to 'x'-axis and found to be 1.31, 1.27, 1.40 and 1.38 eV with respect to the substrate temperature. The variation in optical band gap with increase in substrate temperature might be due to the electron–electron interactions and electron impurity scattering [33].

The electrical parameters such as resistivity (ρ), carrier concentration (n) and mobility (μ) are necessary to determine the electrocatalytic performance of counter electrode materials. The electrical parameters dependency over substrate temperature is represented in Fig.11. The entire CIAS films exhibited p-type semi-conductivity observed from Hall effect experiments at room temperature. The carrier concentration and mobility values lie between $10^{14}$ - $10^{17}$ $cm^3$ and 15-160 $cm^2/Vs$ for the deposited CIAS films. The obtained values are in closer agreement with the thermally evaporated $CuIn_{1-x}Al_xS_2$ films prepared by Cheng et al. [34]. Temperature dependent conductivity measurements (ln σ vs 1000/T (K)) were made using linear four probe method to identify the defect states in CIAS films (Fig.12). It can be observed from the plot that the conductivity of the films increases slowly with the rise in temperature and follows a linear behaviour which means the carriers are non-degenerate. This type of non-degeneracy was observed earlier by Kavitha et al. for SILAR deposited Cu (In Al) $Se_2$ films [35].

The relation between the activation energy ($E_a$) and conductivity (σ) is given by [36],

$$\sigma = \sigma_0 \exp\left(\frac{E_a}{kT}\right) \qquad (6)$$

where 'k' is the Boltzmann constant and 'T' is the temperature and '$\sigma_0$' is the pre-exponential factor. The obtained activation energy values are presented in Table 1. The activation energy values are found to be low due to the occupation of Al atoms in chalcopyrite $CuInS_2$ creating a shallow acceptor level below Cu vacancies [37]. Moreover, the weak dependence of temperature over conductivity reveals that ionized impurity scattering is the dominant mechanism that hinders the carrier transport. The variation in activation energy and high resistivity values

strain and dislocations created in $CuInAlS_2$ films. Similar type of observation was made by Mahendran et al. for Bi doped $CuInS_2$ films [12]. Hence it can be concluded that $CuInAlS_2$ film deposited at 300 °C has the optimized electrical parameters and it is more preferable to the counter electrode in DSSCs.

*3.9. Electrochemical activity and stability of CEs*

The device performance of CIAS CE depends upon the catalytic activity towards tri-iodide reduction [38]. To elucidate the catalytic performance of the CIAS CEs in $I^-/I_3^-$ process, cyclic voltammogram (CV) of all the CEs was studied with iodide containing electrolyte. The CV spectra of CIAS CEs were compared with those of the Pt CE as shown in Fig. 13 (i). A pair of oxidation and reduction peak was observed for all the CIAS CEs predicting that it can act as electrocatalysts for the reduction of $I^-$ to $I_3^-$. In the CV curves, the anodic ($J_{pa}$) and cathodic ($J_{pc}$) peak current densities and peak-to-peak separation ($\Delta E_p$) are the two vital parameters to determine the catalytic activity [39]. The electrocatalytic behavior of the CIAS CE increases with the increasing deposition temperature and further decreases at the higher deposition temperatures. The highest cathodic current density $J_{pc}$ with the lowest $\Delta E_p$ was achieved for the CIAS CE deposited at 300 °C indicating higher electrocatalytic activity in the redox couple as the nanoflake morphology offers high surface area for iodine ions to be diffused over the surface. The advantage of CIAS nanoflake structures over other morphological features is rapid charge transfer at the electrolyte interface [40]. The low $J_{pc}$ obtained for the other CIAS CEs denotes the poor interactions with the electrolyte that led to an increase in the interfacial charge transfer resistance, thereby decreasing the fill factor of the device [41]. The long-term stability of CIAS

delamination or peel off of CIAS CE was observed even after completing 40 cycles which ensures that the nebulizer spray-deposited film is stable and robust in nature in the electrolyte. Figure 13 (ii) shows no variations in anodic and cathodic peak current densities; specifying the more electrocatalytic stability in $I^-/I_3^-$ process and suggesting an alternative CE for Pt.

*3.10. Electrochemical Impedance Spectroscopy (EIS)*

The electron charge transport at the CE/electrolyte interface can be studied by electrochemical impedance spectroscopy. Figure 14 (i) represents the CIAS/CEs with the $TiO_2$ based-DSSCs devices of EIS spectra. The series resistance ($R_s$) and the charge transfer resistance ($R_{ct}$) values of CIAS CEs at the CE/electrolyte interface for $I_3^-$ reduction are listed in Table 2. The $R_s$ and $R_{ct}$ are determined from the horizontal intercept and the radius of semicircle in the high frequency region. The equivalent circuit of CIAS CE fitted by Zsimpwin software was shown in the inset of Fig.14 (ii). The variation observed in $R_s$ value depends on the binding nature with the FTO substrate and electrical resistivity of the films [42]. The minimum value of $R_s$ and $R_{ct}$ was obtained for the CIAS CE prepared at 300 °C and it denotes strong electrocatalytic behaviour and fast electron transfer at the CE/electrolyte interface. The series resistance and charge transfer resistance increases drastically for higher deposition temperatures (350 and 400 °C). The high series resistance ($R_s$) might be attributed to decrease in electrical conductivity and carrier density as well as the grain boundary defects generated during high thermal treatment to the substrate. Larger charge transfer resistance ($R_{ct}$) could be ascribed to the agglomeration of grains and dense nature of the films deposited at elevated substrate temperatures reduces the diffusion of electrolyte ions, thereby impedes the easy charge transfer

higher substrate temperatures would result in low fill factor and efficiency in DSSCs [43].

*3.11. Tafel Analysis*

The Tafel polarization of CIAS CEs with symmetric cells is analyzed to determine the relation between the overpotential and current density, which can get the exchange current density ($J_0$) and limiting diffusion current density ($J_{lim}$). The Tafel polarization curves of CIAS CEs and the limiting diffusion coefficient values are depicted in Fig.14 (ii) and Table 2. The exchange current density $J_0$ and diffusion limit coefficient $J_{lim}$ were determined from the intercept of slope near the origin and the Tafel curve at high potential respectively. The parameters $J_0$ and $J_{lim}$ achieved for the CIAS CE deposited at 300 °C were nearer to that of Pt CE suggesting that CIAS CE can replace the Pt CE.

*3.12. Photocurrent density-voltage (J-V) characterization*

Figure 15 displays the photocurrent density-voltage of CIAS CEs at different substrate temperatures. The photovoltaic parameters like short-circuit current density ($J_{sc}$), open-circuit voltage ($V_{oc}$), fill factor (FF) and efficiency (η) of CIAS CEs are listed in Table 3. The efficiency and FF of Pt CE was about 0.63 and 5.30 %. The decrement in FF for CIAS CEs could be attributed to high series resistance ($R_s$) and charge transfer resistance ($R_{ct}$) compared to Pt electrode [44]. The efficiency obtained at 250 °C was 1.47% owing to the poor electrocatalytic behavior (low $J_{pc}$ and $\Delta E_{PP}$) as witnessed from CV results. Among CIAS CEs, the maximum $J_{sc}$ (7.22 mA/cm$^2$) and efficiency (2.55 %) were attained for the CIAS CE deposited at 300 °C. The nanoflake-like morphology with high electrical conductivity and carrier concentration has

substrate temperatures, the FF and η of CIAS CEs decreased due to the poor crystalline nature, high $R_s$ and $R_{ct}$ values as detected from XRD and EIS analysis. Therefore, the CIAS CE can be used instead of Pt CE in DSSCs by optimizing the parameters in experimental technique and high photo conversion efficiency can be achieved.

## 4. Conclusion

CIAS thin films were prepared by nebulizer spray method for different substrate temperatures. The substrate temperature of CIAS film has a strong influence on the structural, morphological, optical and electrical properties. The better crystalline quality of CIAS thin film was observed at 300 °C with the maximum crystallite size. The nanoflake-like morphology was examined by the SEM analysis. The absorbance spectrum covers broad spectral range in the visible region for all the deposited CIAS films and obtained the optimum band gap energy. The electrical properties of the films were investigated by linear four probe and Hall effect measurements. CIAS thin film used as a CE in DSSCs attained good electrocatalytic activity for reduction of $I_3^-$, charge transfer kinetics and series resistances stating that CIAS CEs has better electrochemical property. To the best of our knowledge, CIAS as a CE in DSSCs has been reported for the first time and achieved the maximum efficiency of 2.55 % with the short-circuit current density of 7.22 mA/cm$^2$. Therefore, CIAS is a promising candidate and paves a new pathway for fabricating low-cost with the high efficient CEs for DSSCs and it can be a better replacement of Pt CE by improving the experimental parameters.

The authors would like to record their sincere thanks to the University Grants Commission, New Delhi for providing financial support through Major Research Project Scheme (MRP) [F.no.42-903/2013(SR)]. The authors also acknowledge Dr. R. Ramesh Babu, Assistant Professor, School of Physics, Bharathidasan University, Tiruchirappalli-24, for extending the Hall measurement facilities established under the DST grant (D.O.No.SR/S2/CMP-35/2004). One of the authors, Dr. S. K. Panda, would like to thank the Department of Science and Technology (DST), Government of India, for the financial support (Project no: SB/FT/CS-048/2012).

[1] Hong Yuan, Qingze Jiao, Shenli Zhang, Yun Zhao, Qin Wu, Hansheng Li, In situ chemical vapor deposition growth of carbon nanotubes on hollow CoFe 2 O 4 as an efficient and low cost counter electrode for dye-sensitized solar cells, J. Power Sources, 325 (2016) 417-426.
[2] Jinghao Huo, Min Zheng, Yongguang Tu, Jihuai Wu, Linhua Hu, Songyuan Dai, A high performance cobalt sulfide counter electrode for dye-sensitized solar cells, Electrochim. Acta, 159 (2015) 166-173.
[3] Sara Thomas, TG Deepak, GS Anjusree, TA Arun, Shantikumar V Nair, A Sreekumaran Nair, A review on counter electrode materials in dye-sensitized solar cells, Journal of Materials Chemistry A, 2 (2014) 4474-4490.
[4] Shan-Long Chen, Jie Tao, Hai-Jun Tao, Yi-Zhou Shen, Tao Wang, Lei Pan, High-performance and low-cost dye-sensitized solar cells based on kesterite Cu 2 ZnSnS 4 nanoplate arrays on a flexible carbon cloth cathode, J. Power Sources, 330 (2016) 28-36.
[5] Reshma K Bhosale, Shruti A Agarkar, Ishita Agrawal, Rounak A Naphade, Satishchandra Ogale, Nanophase CuInS 2 nanosheets/CuS composite grown by the SILAR method leads to high performance as a counter electrode in dye sensitized solar cells, Rsc Advances, 4 (2014) 21989-21996.
[6] Lidan Wang, Jianxin He, Mengjuan Zhou, Shuyuan Zhao, Qian Wang, Bin Ding, Copper indium disulfide nanocrystals supported on carbonized chicken eggshell membranes as efficient counter electrodes for dye-sensitized solar cells, J. Power Sources, 315 (2016) 79-85.
[7] Erkan Aydin, Mehmet Sankir, Nurdan Demirci Sankir, Conventional and rapid thermal annealing of spray pyrolyzed copper indium gallium sulfide thin films, J. Alloys Compd., 615 (2014) 461-468.
[8] F Smaili, M Kanzari, B Rezig, Characterization of CuIn 1− x AlxS 2 thin films prepared by thermal evaporation, Materials Science and Engineering: C, 28 (2008) 954-958.
[9] J Olejníček, LE Flannery, SA Darveau, CL Exstrom, Š Kment, NJ Ianno, RJ Soukup, CuIn 1− x Al x S 2 thin films prepared by sulfurization of metallic precursors, J. Alloys Compd., 509 (2011) 10020-10024.
[10] Johanna D Burnett, Olivier Gourdon, Kulugammana GS Ranmohotti, Nathan J Takas, Honore Djieutedjeu, Pierre FP Poudeu, Jennifer A Aitken, Structure–property relationships along the Fe-substituted CuInS 2 series: Tuning of thermoelectric and magnetic properties, Mater. Chem. Phys., 147 (2014) 17-27.
[11] C Mahendran, N Suriyanarayanan, Synthesis and characterization of sprayed Zn-doped polycrystalline CuInS 2 thin films, Optik-International Journal for Light and Electron Optics, 124 (2013) 5089-5094.
[12] C Mahendran, N Suriyanarayanan, Influence of mole concentration on nano crystalline Bi-doped CuInS 2 thin films with the temperature by chemical spray method, Optik-International Journal for Light and Electron Optics, 126 (2015) 4237-4242.
[13] Björn Marsen, Lars Steinkopf, Abhishek Singh, Helena Wilhelm, Iver Lauermann, Thomas Unold, Roland Scheer, Hans-Werner Schock, Effects of Ti-incorporation in CuInS 2 solar cells, Sol. Energy Mater. Sol. Cells, 94 (2010) 1730-1733.
[14] Lingling Xiao, Jun Zhu, Tiezhu Ding, Yanlai Wang, Yue Fan, Qingrui Bo, Synthesis and characterization of Ce-incorporated CuInS 2 chalcopyrites, Mater. Lett., 159 (2015) 392-394.

(2006) 125-129.
[16] N Kamoun Allouche, N Jebbari, C Guasch, N Kamoun Turki, Influence of aluminum doping in CuInS 2 prepared by spray pyrolysis on different substrates, J. Alloys Compd., 501 (2010) 85-88.
[17] N Jebbari, B Ouertani, M Ramonda, C Guasch, N Kamoun Turki, R Bennaceur, Structural and Morphological studies of deposited by spray on various substrates, Energy Procedia, 2 (2010) 79-89.
[18] Ching-Hwa Ho, Single crystal growth and characterization of copper aluminum indium disulfide chalcopyrites, J. Cryst. Growth, 317 (2011) 52-59.
[19] R Kaigawa, A Neisser, R Klenk, M-Ch Lux-Steiner, Improved performance of thin film solar cells based on Cu (In, Ga) S 2, Thin Solid Films, 415 (2002) 266-271.
[20] Sanjay S Latthe, P Sudhagar, C Ravidhas, A Jennifer Christy, D David Kirubakaran, R Venkatesh, Anitha Devadoss, C Terashima, K Nakata, Akira Fujishima, Self-cleaning and superhydrophobic CuO coating by jet-nebulizer spray pyrolysis technique, CrystEngComm, 17 (2015) 2624-2628.
[21] C. Ravi Dhas, A Jennifer Christy, R. Venkatesh, K.S. Anuratha, K. Ravichandran, A. Moses Ezhil Raj, B. Subramanian, Subhendu K. Panda, Nebulizer spray-deposited CuInGaS2 thin films, a viable candidate for counter electrode in dye-sensitized solar cells, Solar energy, 157 (2017) 58-70.
[22] C Ravi Dhas, R Venkatesh, D David Kirubakaran, J Princy Merlin, B Subramanian, A Moses Ezhil Raj, Electrochemical sensing of glucose and photocatalytic performance of porous Co 3 O 4 films by nebulizer spray technique, Mater. Chem. Phys., 186 (2017) 561-573.
[23] C Ravidhas, A Juliat Josephine, P Sudhagar, Anitha Devadoss, C Terashima, K Nakata, Akira Fujishima, A Moses Ezhil Raj, C Sanjeeviraja, Facile synthesis of nanostructured monoclinic bismuth vanadate by a co-precipitation method: structural, optical and photocatalytic properties, Mater. Sci. Semicond. Process., 30 (2015) 343-351.
[24] P Dhamodharan, C Manoharan, S Dhanapandian, P Venkatachalam, Dye-sensitized solar cell using sprayed ZnO nanocrystalline thin films on ITO as photoanode, Spectrochimica Acta Part A: Molecular and Biomolecular Spectroscopy, 136 (2015) 1671-1678.
[25] C Mahendran, N Suriyanarayanan, Effect of zinc doping and temperature on the properties of sprayed CuInS 2 thin films, Mater. Sci. Semicond. Process., 15 (2012) 522-530.
[26] C. Ravi Dhas, R. Venkatesh, R. Sivakumar, A. Moses Ezhil Raj, C. Sanjeeviraja, Effect of solution molarity on optical dispersion energy parameters and electrochromic performance of Co3O4 films, Opt. Mater., 72 (2017) 717-729.
[27] A Moses Ezhil Raj, KC Lalithambika, VS Vidhya, G Rajagopal, A Thayumanavan, M Jayachandran, C Sanjeeviraja, Growth mechanism and optoelectronic properties of nanocrystalline In 2 O 3 films prepared by chemical spray pyrolysis of metal-organic precursor, Physica B: Condensed Matter, 403 (2008) 544-554.
[28] Shanlong Chen, Aichun Xu, Jie Tao, Haijun Tao, Yizhou Shen, Lumin Zhu, Jiajia Jiang, Tao Wang, Lei Pan, In-Situ and Green Method To Prepare Pt-Free Cu2ZnSnS4 (CZTS) Counter Electrodes for Efficient and Low Cost Dye-Sensitized Solar Cells, ACS Sustainable Chemistry & Engineering, 3 (2015) 2652-2659.
[29] R Swapna, MC Santhosh Kumar, The role of substrate temperature on the properties of nanocrystalline Mo doped ZnO thin films by spray pyrolysis, Ceram. Int., 38 (2012) 3875-3883.

preparation of hierarchical nanostructured CuInS 2 counter electrodes for dye-sensitized solar cells, Materials Research Express, 4 (2017) 125001.
[31] Sanjaya D Perera, Haitao Zhang, Xiaoyue Ding, Andrew Nelson, Richard D Robinson, Nanocluster seed-mediated synthesis of CuInS 2 quantum dots, nanodisks, nanorods, and doped Zn-CuInGaS 2 quantum dots, Journal of Materials Chemistry C, 3 (2015) 1044-1055.
[32] Tina Sebastian, Manju Gopinath, C Sudha Kartha, KP Vijayakumar, T Abe, Y Kashiwaba, Role of substrate temperature in controlling properties of sprayed CuInS 2 absorbers, Solar energy, 83 (2009) 1683-1688.
[33] S Marikkannu, M Kashif, N Sethupathy, VS Vidhya, Shakkthivel Piraman, A Ayeshamariam, M Bououdina, Naser M Ahmed, M Jayachandran, Effect of substrate temperature on indium tin oxide (ITO) thin films deposited by jet nebulizer spray pyrolysis and solar cell application, Mater. Sci. Semicond. Process., 27 (2014) 562-568.
[34] Kong-Wei Cheng, Miao-Syuan Fan, Preparation and characterization of CuInxAl1−xS2 films using the sulfurization of metal precursors for photoelectrochemical applications, Journal of the Taiwan Institute of Chemical Engineers, 44 (2013) 407-414.
[35] B Kavitha, M Dhanam, Transport properties of copper indium aluminum selenide thin films deposited by successive Ionic layer adsorption and reaction, Mater. Sci. Semicond. Process., 16 (2013) 495-503.
[36] C Ravi Dhas, A Jennifer Christy, R Venkatesh, D David Kirubakaran, R Sivakumar, K Ravichandran, A Moses Ezhil Raj, C Sanjeeviraja, Effect of sputtering power on properties and photovoltaic performance of CIGS thin film solar cells, Mater. Res. Innovations, 21 (2017) 286-293.
[37] JM Peza-Tapia, VM Sanchez-Resendiz, ML Albor-Aguilera, JJ Cayente-Romero, LR De Leon-Gutierrez, M Ortega-Lopez, Electrical and optical characterization of Na: CuInS 2 thin films grown by spray pyrolysis, Thin Solid Films, 490 (2005) 142-145.
[38] S Nagarajan, P Sudhagar, V Raman, Woohyung Cho, KS Dhathathreyan, Yong Soo Kang, A PEDOT-reinforced exfoliated graphite composite as a Pt-and TCO-free flexible counter electrode for polymer electrolyte dye-sensitized solar cells, Journal of Materials Chemistry A, 1 (2013) 1048-1054.
[39] Zhiwei Shi, Hao Lu, Qiong Liu, Fengren Cao, Jun Guo, Kaimo Deng, Liang Li, Efficient p-type dye-sensitized solar cells with all-nano-electrodes: NiCo2S4 mesoporous nanosheet counter electrodes directly converted from NiCo2O4 photocathodes, Nanoscale research letters, 9 (2014) 608.
[40] Hee-Je Kim, Byeonghun Ko, Chandu VVM Gopi, Mallineni Venkata-Haritha, Young-Seok Lee, Facile synthesis of morphology dependent CuS nanoparticle thin film as a highly efficient counter electrode for quantum dot-sensitized solar cells, J. Electroanal. Chem., 791 (2017) 95-102.
[41] Julian Burschka, Vincent Brault, Shahzada Ahmad, Livain Breau, Mohammad K Nazeeruddin, Benoît Marsan, Shaik M Zakeeruddin, Michael Grätzel, Influence of the counter electrode on the photovoltaic performance of dye-sensitized solar cells using a disulfide/thiolate redox electrolyte, Energy & Environmental Science, 5 (2012) 6089-6097.
[42] Krishnaiah Mokurala, Sudhanshu Mallick, Effect of annealing atmosphere on quaternary chalcogenide-based counter electrodes in dye-sensitized solar cell performance: synthesis of

[43] Abhik Banerjee, Kush Kumar Upadhyay, Sumit Bhatnagar, Mukta Tathavadekar, Umesh Bansode, Shruti Agarkar, Satishchandra B Ogale, Nickel cobalt sulfide nanoneedle array as an effective alternative to Pt as a counter electrode in dye sensitized solar cells, Rsc Advances, 4 (2014) 8289-8294.
[44] S Srinivasa Rao, Chandu VVM Gopi, Soo-Kyoung Kim, Min-Kyu Son, Myeong-Soo Jeong, A Dennyson Savariraj, K Prabakar, Hee-Je Kim, Cobalt sulfide thin film as an efficient counter electrode for dye-sensitized solar cells, Electrochim. Acta, 133 (2014) 174-179.

**Figure 1: X-ray diffraction of CIAS thin films at different substrate temperatures**

**Figure 2: Substrate temperature vs crystallite size, strain and dislocation density of CIAS thin films**

**Figure 3: Substrate temperature vs tetragonal c/a ratio and FWHM**

**Figure 4: Raman Spectra of CIAS thin films at different substrate temperatures**

**Figure 5: SEM images of CIAS thin films at different substrate temperatures**

**Figure 6: AFM images of CIAS thin films at different substrate temperatures**

**Figure 7: (i) Survey spectrum and (ii) Core level spectra of Cu, In, Al and S of CIAS thin film deposited at 300 °C**

**Figure 8: Energy Dispersive X-ray Analysis spectra of CIAS thin film at 300 °C**

**Figure 9: Absorbance vs wavelength of CIAS thin films at different substrate temperatures**

**Figure 10: Optical band gap of CIAS thin films at different substrate temperatures**

**Figure 11: Electrical parameters of CIAS thin films deposited at different substrate temperatures**

**Figure 12: Arrhenius plot (ln σ vs. 1000/T ($K^{-1}$)) of CIAS films at different substrate temperatures**

**Figure 13: (i) Cyclic voltammograms of Pt and CIAS CEs and (ii) 40 continuous cyclic voltammograms of CIAS CE deposited at 300 °C**

**Figure 14: (i) EIS spectra of the $TiO_2$ based DSSCs devices with Pt and CIAS CEs and (ii) Tafel polarization of Pt and CIAS symmetric cells**

**Figure 15: J – V characteristics of DSSCs with Pt and different CIAS CEs**

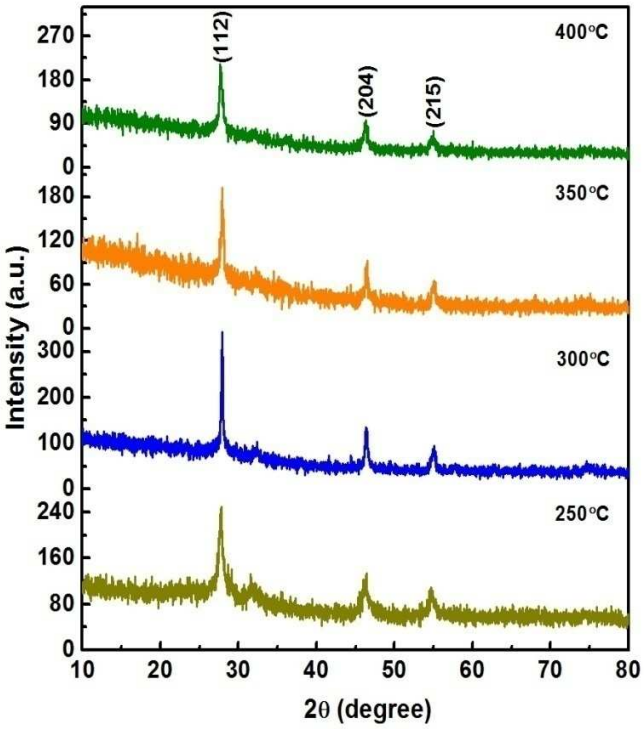
(112)
(204)
(215)
400°C
350°C
300°C
250°C
Intensity (a.u.)
2θ (degree)
270
180
90
0
180
120
60
0
300
200
100
0
240
160
80
0
10
20
30
40
50
60
70
80

**Figure 1**

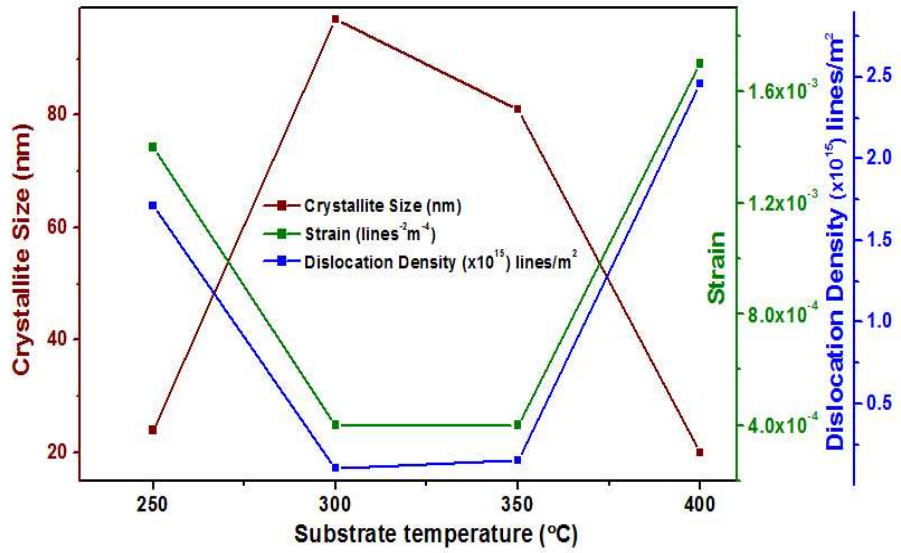


**Figure 2**

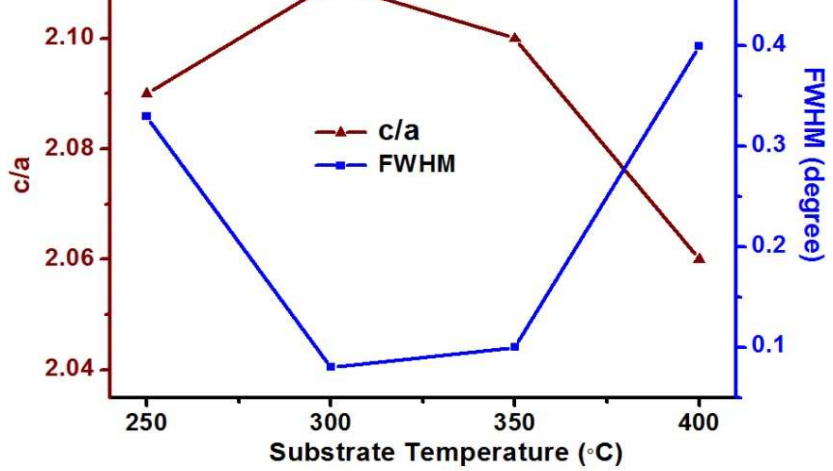


**Figure 3**

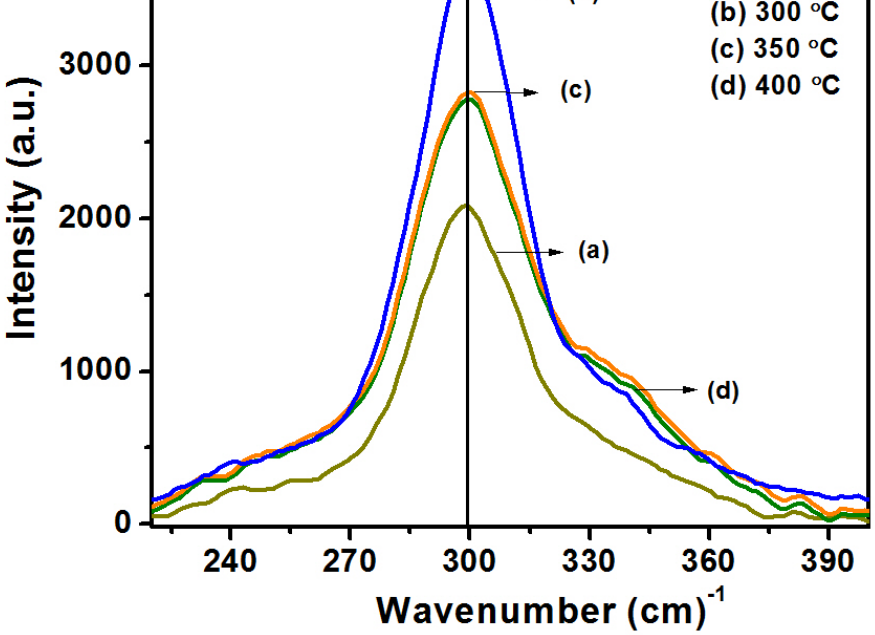


**Figure 4**

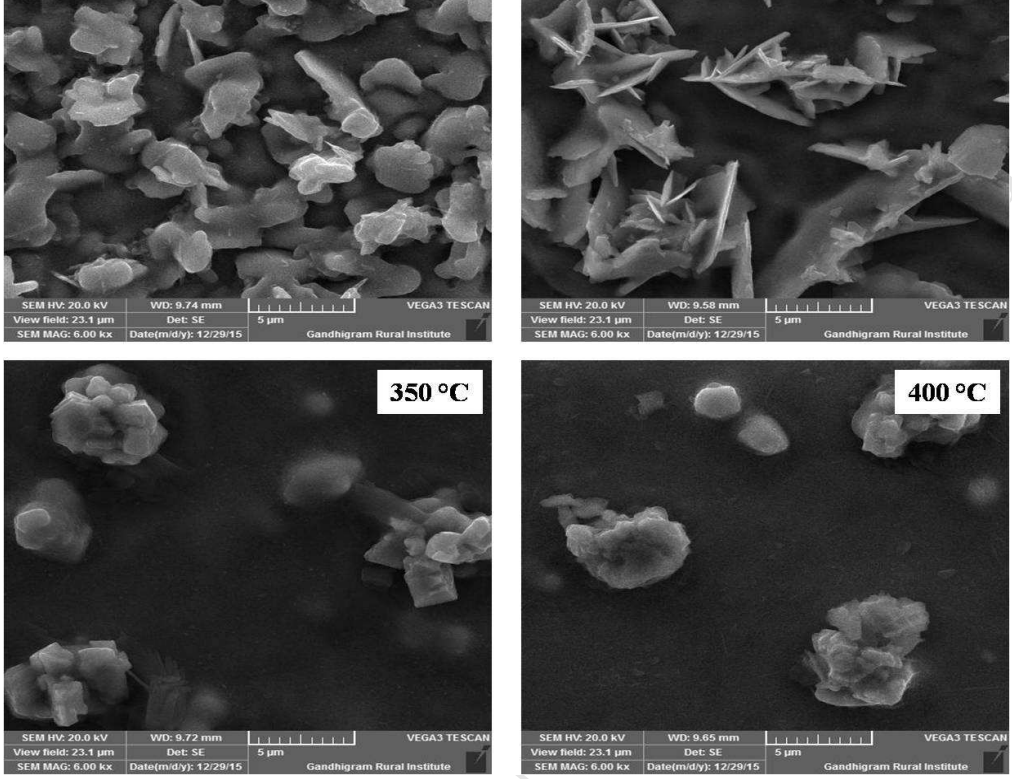


**Figure 5**

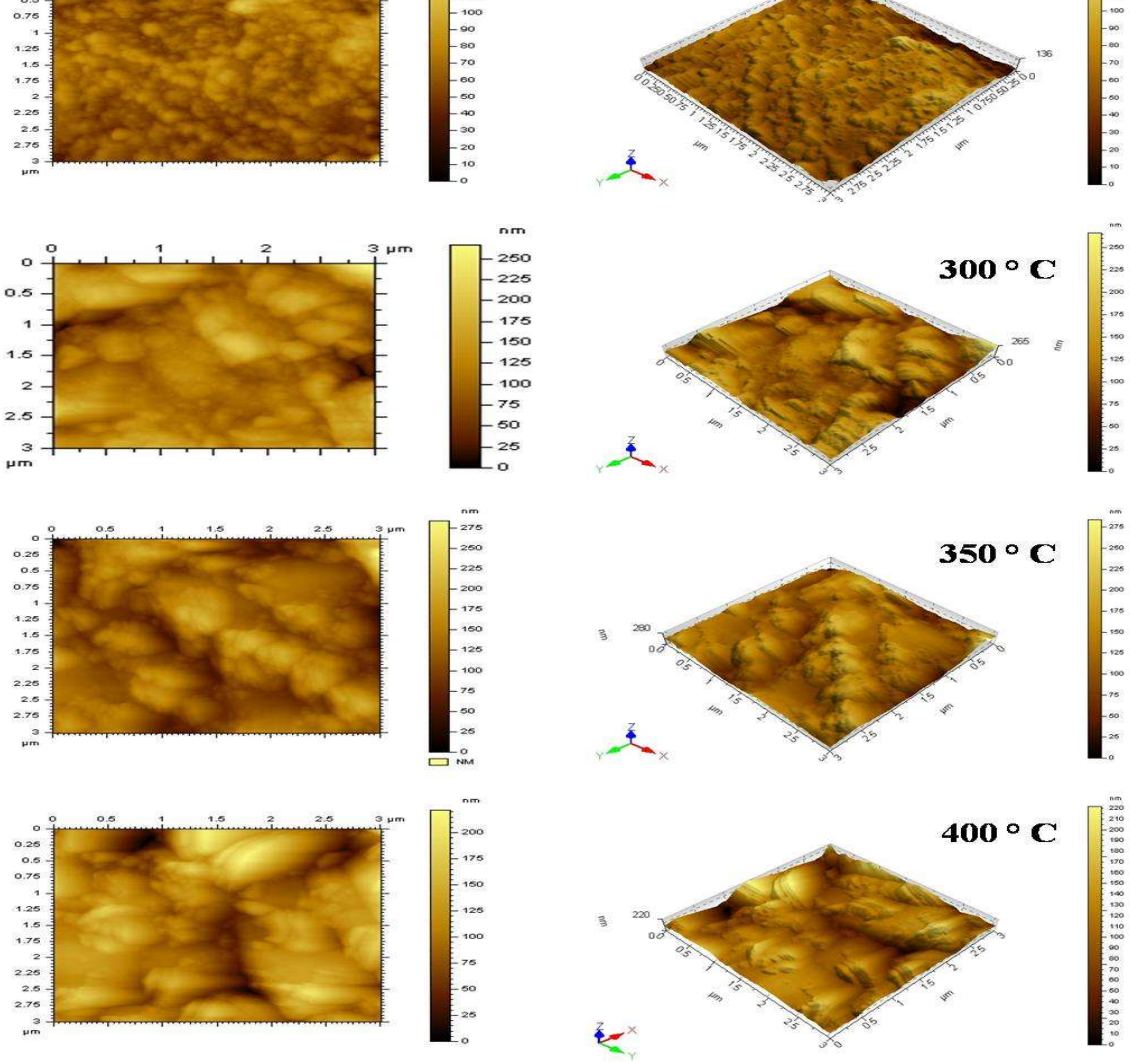


**Figure 6**

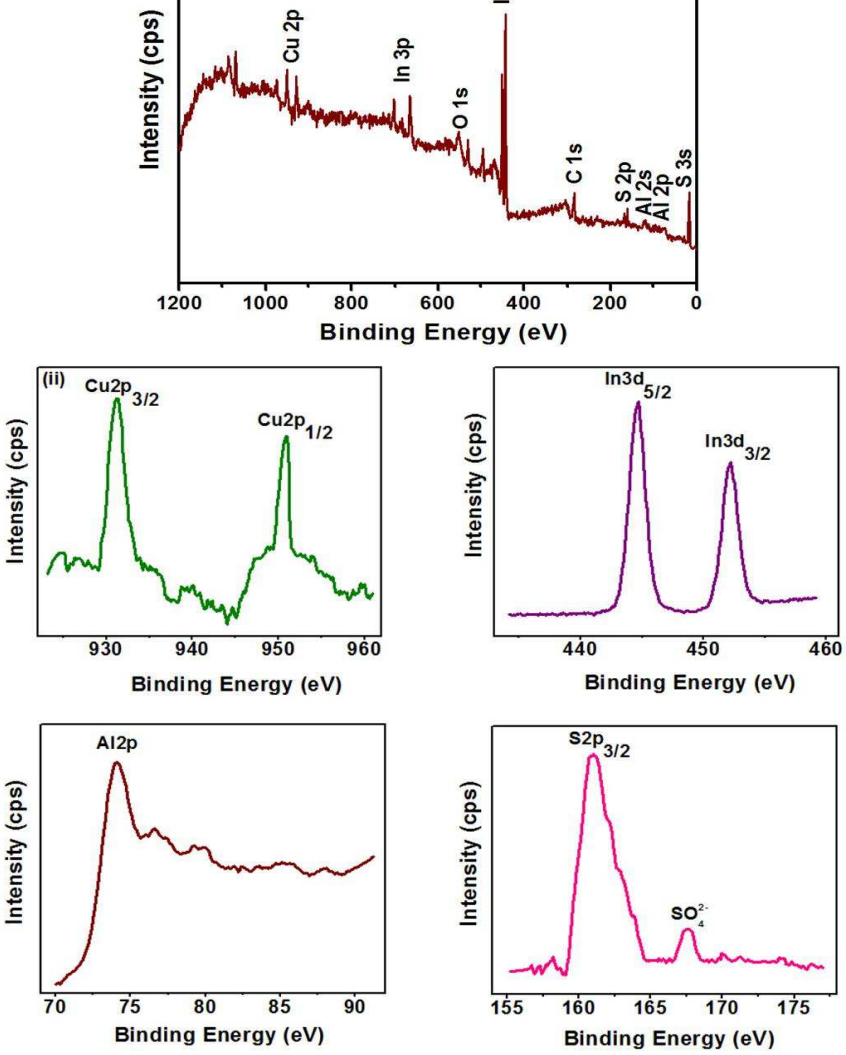


**Figure 7**

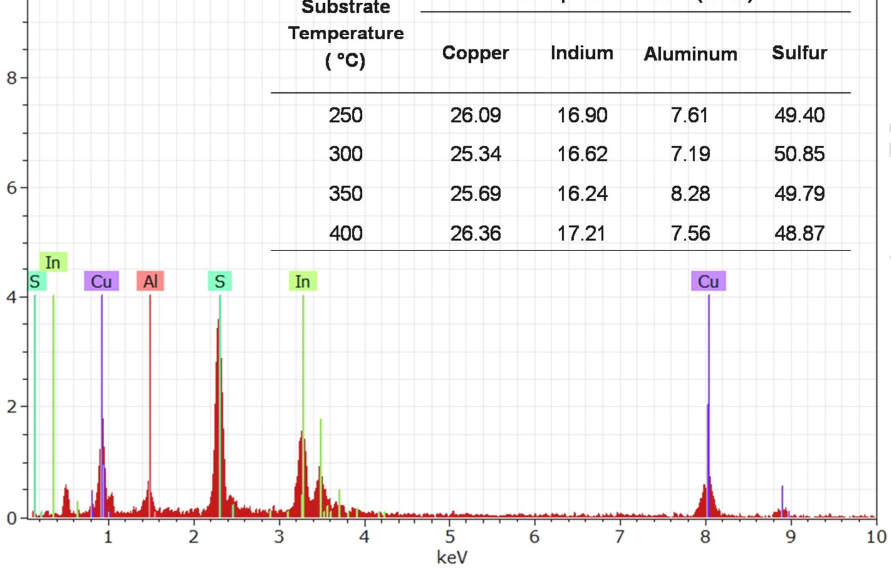


| Substrate Temperature ( °C) | Copper | Indium | Aluminum | Sulfur |
|---|---|---|---|---|
| 250 | 26.09 | 16.90 | 7.61 | 49.40 |
| 300 | 25.34 | 16.62 | 7.19 | 50.85 |
| 350 | 25.69 | 16.24 | 8.28 | 49.79 |
| 400 | 26.36 | 17.21 | 7.56 | 48.87 |

**Figure 8**

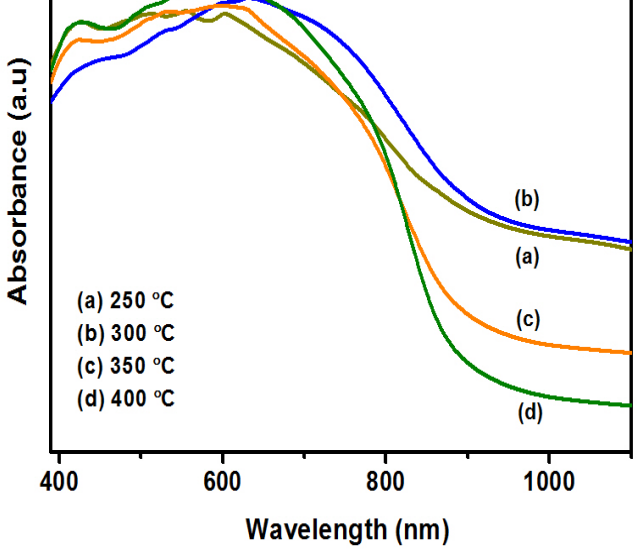


**Figure 9**

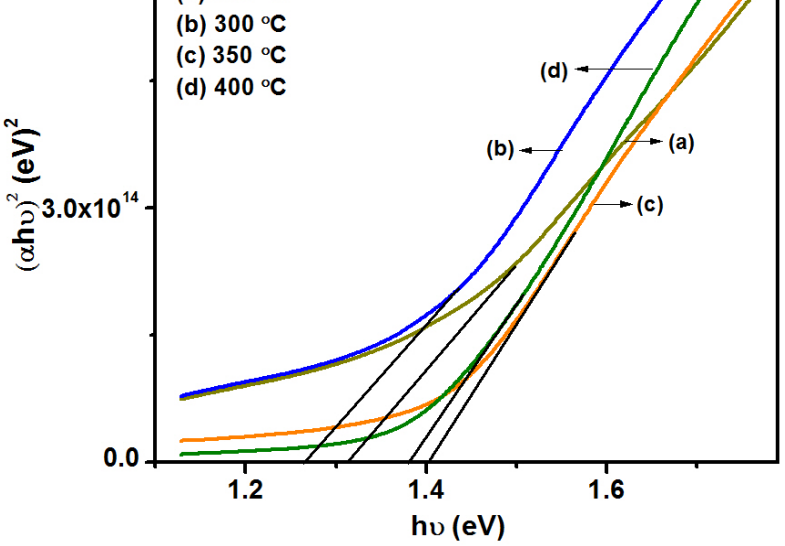


**Figure 10**

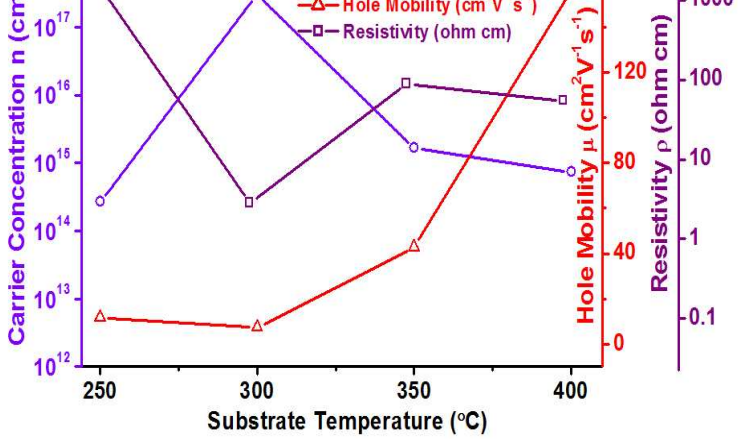


**Figure 11**

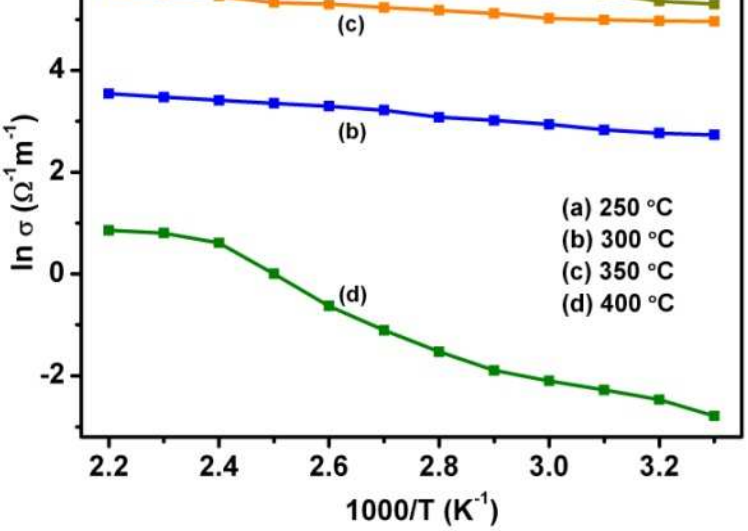


**Figure 12**

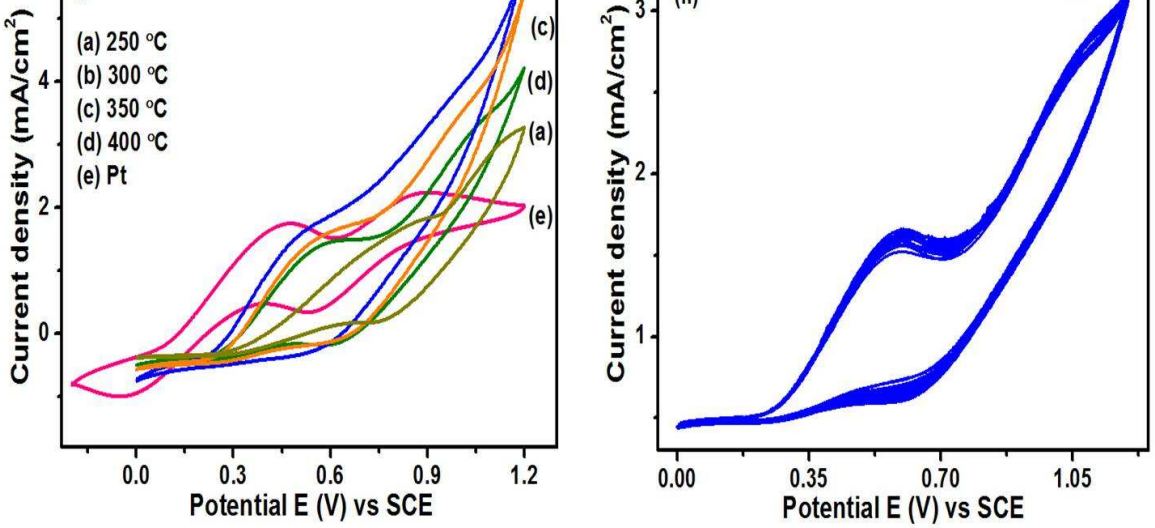


**Figure 13**

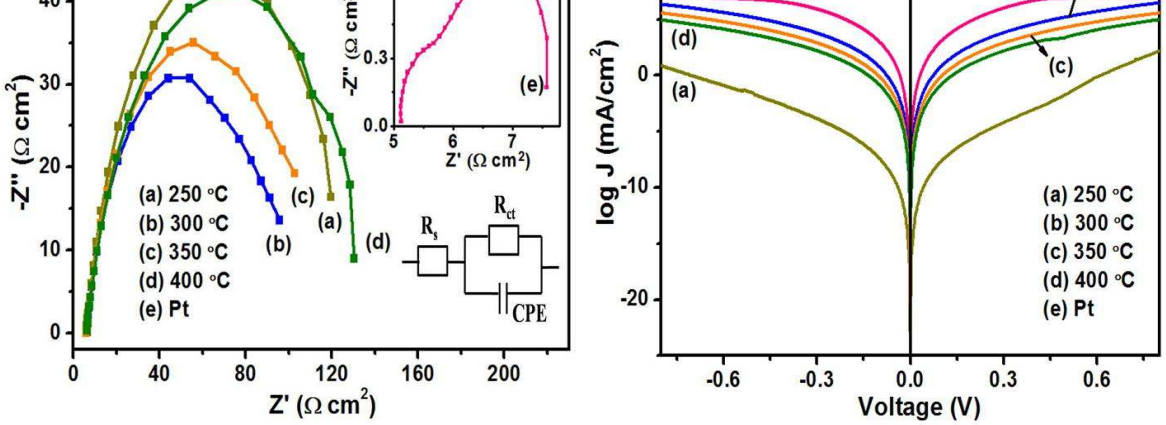


**Figure 14**

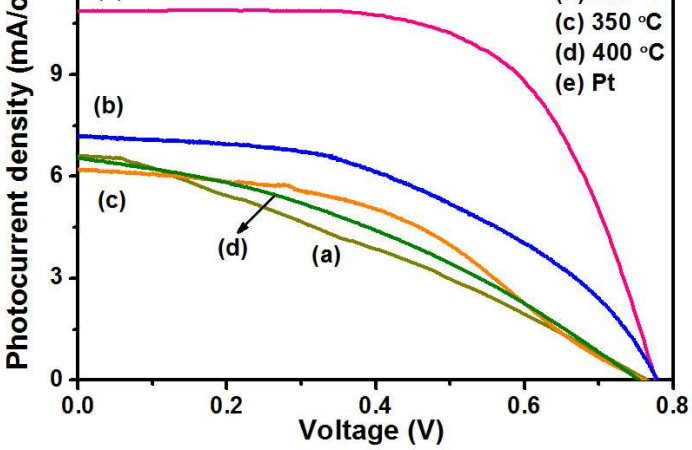


**Figure 15**

**Table 1: Lattice Constants, Root Mean Square Roughness and Activation Energy of CIAS thin films**

| Substrate Temperature (°C) | Lattice Constants (Å) | | Root Mean Square Roughness (nm) | Activation Energy $E_a$ (eV) |
|---|---|---|---|---|
| | a | c | | |
| 250 | 5.49 | 11.47 | 32.5 | 0.10 |
| 300 | 5.45 | 11.48 | 23.3 | 0.19 |
| 350 | 5.46 | 11.44 | 32.0 | 0.11 |
| 400 | 5.53 | 11.37 | 35.6 | 0.34 |

| Samples | $J_{pa}$ (mA/cm$^2$) | $J_{pc}$ (mA/cm$^2$) | $\Delta E_p$ (mV) | $R_s$ (Ω cm$^2$) | $R_{ct}$ (Ω cm$^2$) | log $J_{lim}$ (mA/cm$^2$) |
|---|---|---|---|---|---|---|
| Pt | 1.75 | -1.00 | 421 | 5.12 | 2.46 | 7.14 |
| 250 °C | 1.42 | -0.32 | 469 | 6.49 | 113.01 | 2.22 |
| 300 °C | 1.63 | -0.57 | 436 | 6.02 | 89.50 | 6.42 |
| 350 °C | 1.54 | -0.50 | 448 | 6.14 | 96.63 | 5.51 |
| 400 °C | 1.45 | -0.42 | 455 | 6.21 | 124.09 | 4.93 |

| Samples | $V_{oc}$ (V) | $J_{sc}$ (mA/cm$^2$) | FF | η (%) |
|---|---|---|---|---|
| Pt | 0.78 | 10.87 | 0.63 | 5.30 |
| 250 °C | 0.76 | 6.60 | 0.29 | 1.47 |
| 300 °C | 0.78 | 7.22 | 0.45 | 2.55 |
| 350 °C | 0.76 | 6.19 | 0.43 | 2.03 |
| 400 °C | 0.75 | 6.56 | 0.36 | 1.75 |